

# A Graph-Based Reinforcement Learning Approach with Frontier Potential Based Reward for Safe Cluttered Environment Exploration

Gabriele Calzolari, Vidya Sumathy, Christoforos Kanellakis, George Nikolakopoulos

**Abstract**—Autonomous exploration of cluttered environments requires efficient exploration strategies that guarantee safety against potential collisions with unknown random obstacles. This paper presents a novel approach combining a graph neural network-based exploration greedy policy with a safety shield to ensure safe navigation goal selection. The network is trained using reinforcement learning and the proximal policy optimization algorithm to maximize exploration efficiency while reducing the safety shield interventions. However, if the policy selects an infeasible action, the safety shield intervenes to choose the best feasible alternative, ensuring system consistency. Moreover, this paper proposes a reward function that includes a potential field based on the agent’s proximity to unexplored regions and the expected information gain from reaching them. Overall, the approach investigated in this paper merges the benefits of the adaptability of reinforcement learning-driven exploration policies and the guarantee ensured by explicit safety mechanisms. Extensive evaluations in simulated environments demonstrate that the approach enables efficient and safe exploration in cluttered environments.

## I. INTRODUCTION

Efficient and safe exploration in cluttered environments, such as forests, poses significant challenges for autonomous robotic systems. These challenges encompass optimal path planning, uniform coverage, and ensuring safety during decision-making. Traditional exploration strategies, such as random exploration and frontier-based approaches, are often inadequate in real-world environments since they lack adaptability to evolving scenarios, suboptimal path planning, and take myopic decisions. On the other hand, Reinforcement Learning (RL)-based policies enable adaptive decision-making by optimizing long-term rewards and dynamically responding to environmental changes. Among these learning-based methods, Graph Neural Network (GNN)-based architectures have gained increasing attention due to their ability to represent spatial relationships within an environment using graph structures, allowing policies to extract and leverage meaningful features from critical locations in the scene when making navigation decisions. Unlike classical strategies, learned policies provide limited insight into the decision-making process and offer no explicit guarantees that they have acquired the correct behavior beyond statistical evaluation in testing environments. This issue is especially

critical in safety-sensitive applications, where an agent must demonstrably adhere to strict constraints to prevent hazardous behavior. To address this, recent research is focusing on integrating safety mechanisms into RL-based frameworks, ensuring compliance with safety constraints while maintaining adaptability. One promising direction involves combining deep learning methods, capable of encoding complex behaviors, with safety filters that impose hard constraints on action selection, thereby preventing unsafe decisions. This hybrid approach enhances the robustness and reliability of learned policies, facilitating their deployment in real-world environments.

### A. Related Works

Recent advancements in reinforcement learning have significantly affected autonomous robotic exploration enabling agents to efficiently and safely explore cluttered environments [1]–[6]. In particular, [7] proposes a Unmanned Aerial Vehicle (UAV) navigation method using Deep Reinforcement Learning (DRL) with a stochastic value function, modeling navigation as a partially observable Markov decision process and employing the fast recurrent stochastic valued gradient algorithm for safe exploration in large, cluttered 3D environments. The approach proposed in [8] integrates TD3-based DRL with global waypoint selection for autonomous goal-driven exploration, avoiding local optima without prior maps or human input. On the other hand, [9] proposes ARiADNE, an attention-based DRL approach, that enables real-time, non-myopic path planning by learning spatial dependencies and predicting exploration gains. The work [10] proposes ReLMM that autonomously teaches robots navigation and grasping via RL, using modular policies, uncertainty-driven exploration, and autonomous resets. A recent trend is to use Graph Neural Network with reinforcement learning [11]–[13] to implement the exploration policies since these models can effectively leverage the spatial relationships between relevant locations in the environment. While [14] introduces a DRL-based Spatiotemporal Neural Network on Graph for efficient exploration, leveraging past trajectories, obstacles, and waypoints to estimate optimal targets, [15] presents a GNN approach for autonomous exploration, generalizing across graph topologies while ensuring high performance in explored volume. The work in [16] introduces SGRL, a GNN-based deep Q-learning algorithm for autonomous driving decisions, leveraging agent interactions. A reinforcement learning-based visual navigation framework MGRL is proposed in [17], that models uncertainty with a Markov network, uses GNN for inference, and integrates knowledge

This work was partially supported by the Wallenberg AI, Autonomous Systems and Software Program (WASP) funded by the Knut and Alice Wallenberg Foundation, and by the European Union’s Horizon Europe Research and Innovation Program, under the Grant Agreement No. 101119774 SPEAR.

The authors are within the Robotics and AI Group, Department of Computer Science, Electrical and Space Engineering, Luleå University of Technology, Sweden. Corresponding author’s e-mail: gabcal@ltu.se



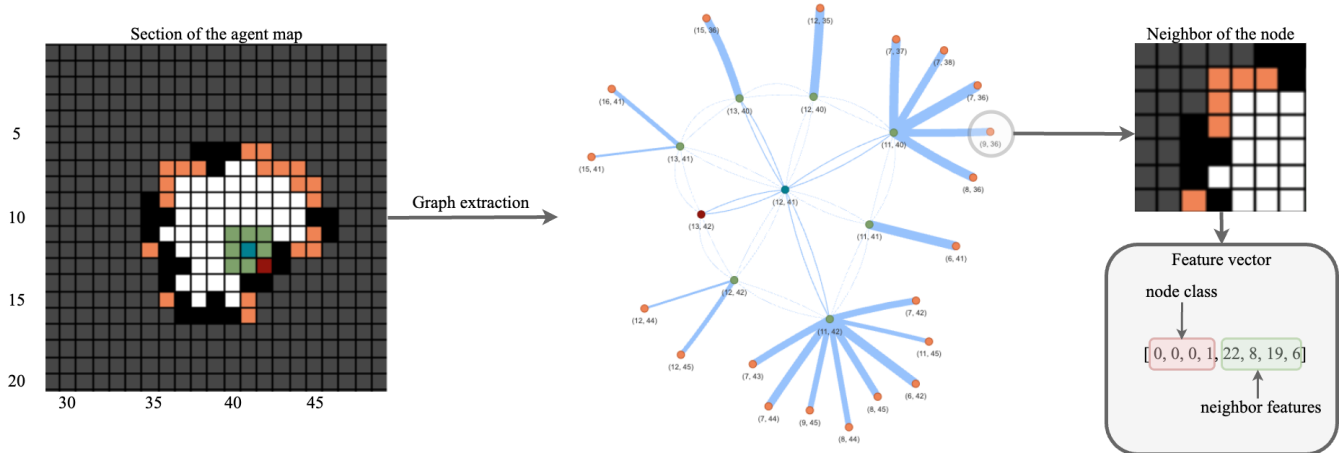


Fig. 2. Illustration of the exploration graph extraction, used as observation  $o_t$ , representing the agent’s exploration map. The image depicts a section of the known arena with occupied (black), unknown (gray), and free (white) cells. The agent’s position, feasible and unfeasible next-step navigation goals, and frontiers are marked in blue, green, red, and orange, respectively. The graph structure captures node relationships, while the right side highlights a frontier’s local neighborhood and its extracted feature vector. Moreover, the graph’s edge thickness is proportional to the distance between connected nodes.

is then computed for the agent’s policy, incorporating the agent’s position, navigation goals, and the border between traversable and unknown regions, as detailed in II-B. As in Fig. 1, the proposed agent’s policy combines a greedy policy  $\pi_\theta(o_t)$  that select a movement  $a_t^\pi \in \mathcal{A}$  towards one of the eight neighboring cells and a safety shield  $\sigma(a_t^\pi)$  hard-constrained to prevent unfeasible actions. In particular, it can confirm the action  $a_t^\pi$  if it is feasible according to the agent’s observation  $o_t$ , otherwise it chooses an action belonging to the feasible action set  $\mathcal{A}_t^f \subseteq \mathcal{A}$ , containing only those actions not leading to collision with obstacles, that is more similar to  $a_t^\pi$ . The GNN-based policy  $\pi_\theta$  is trained via reinforcement learning to maximize the expansion of  $\mathcal{M}_t^a$  while minimizing unfeasible actions  $a_t^\pi$  that require intervention from the safety shield  $\sigma$ . The action filtered by the safety shield  $a_t^\sigma$  is then used to move the agent to a new location, and this process repeats until either the exploration ratio  $\rho_t \geq \rho^*$  or the number of iterations  $n_s \geq n_s^*$ , where  $\rho^*$  and  $n_s^*$  are the exploration threshold and the maximum number of the agent’s interactions with the environment.

The exploration greedy policy  $\pi_\theta$  is trained using the Policy Proximal Optimization (PPO) [30] algorithm and a critic network  $V_\phi$  is included as described in II-C. At each step, the reward  $r(s_t, a_t^\pi, a_t^\sigma, s_{t+1})$ , where  $s_t$  and  $s_{t+1}$  represent the agent’s position and exploration discoveries before and after action  $a_t^\sigma$ , is generated by the environment and returned to the agent’s policy.

### B. Graph-based Agent’s Observation

The agent’s observation  $o_t$  at time  $t$  is an exploration graph  $\mathcal{G} = (\mathcal{V}, \mathcal{E})$ , where nodes  $\mathcal{V}$  represent the agent’s position  $v_a^a$ , neighboring cells  $\mathcal{V}_n$ , and frontiers  $\mathcal{V}_f$ , while edges  $\mathcal{E}$  encode spatial relations with both undirected and bidirected connections, as shown in Fig. 2. In particular,  $\mathcal{E}$  includes edges bi-connecting the agent node  $v_a$  to each possible next-step waypoint  $v_n \in \mathcal{V}_n$ . Moreover, bidirectional connections between the nodes in  $\mathcal{V}_n$  are also added according to Eq. (1).

$$\mathcal{E}_n = \{\langle v_n, v_m \rangle \mid v_n, v_m \in \mathcal{V}_n, \|v_n - v_m\|_\infty \leq 1\} \quad (1)$$

where  $\|\cdot\|_\infty$  is the Chebyshev norm. Furthermore, each frontier node  $v_f \in \mathcal{V}_f$  is connected to its nearest navigation node  $v_n^*$ , linking unexplored regions to waypoints according to  $\mathcal{E}_f = \{\langle v_f, v_n^* \rangle \mid v_f \in \mathcal{V}_f\}$  where  $v_n^*$  is given by Eq. 2.

$$v_n^* = \arg \min_{v_n \in \mathcal{V}_n} \|v_f - v_n\|_2, \quad (2)$$

Each edge is weighted by the Euclidean distance between its nodes, and each node  $v_i$  has a feature vector  $\mathbf{x}_{v_i} \in \mathbb{R}^8$  encoding the node class and local environment features extracted from the agent’s map  $\mathcal{M}_t^a$ . In particular, the first four dimensions of the node feature vector use one-hot encoding, a method for converting categorical variables into a binary format, to define if it is the agent node, a traversable or non-traversable next-step navigation node or a frontier node. Furthermore, each node  $v_i$  encodes local occupancy statistics from a  $k \times k$  neighborhood, summarizing the number of free, unknown, occupied, and frontier cells around the node  $v_i$  according to the agent’s map  $\mathcal{M}_t^a$  as illustrated in Fig. 2.

### C. Architecture of the Greedy Exploration Policy and Critic

Both the exploration greedy policy  $\pi_\theta(o_t)$  and the critic network  $V_\phi$  are implemented as multi-head attention-based graph neural networks leveraging two sequential GATv2Conv [31] layers that use attention mechanisms to compute node representations by considering both node

TABLE I  
HYPERPARAMETERS OF THE LAYERS IN THE GRAPH NEURAL NETWORKS

GATv2Conv	Input Dim	Output Dim	Heads	Activation
Layer 1	8	16	4	ReLU
Layer 2	64	1	1	None

features and edges. In particular, the first layer has hyperparameters shown in Table I and 4 parallel attention heads to transform node features into a concatenated higher-dimensional hidden representation according to Eq. (3)

$$\mathbf{x}_{v_i}^{(1)} = \oplus_{h=1}^4 \left( \sum_{v_j \in \mathcal{N}(v_i) \cup \{v_i\}} \alpha_{v_i, v_j}^h \Theta_t^h \mathbf{x}_{v_j} \right) \quad (3)$$

where  $\Theta_t^h$  is the learned transformation matrix for target nodes from head  $h$ ,  $\mathcal{N}(v_i)$  denotes the neighbors of node  $v_i$ ,  $\oplus$  stands for the concatenation operator and the adaptive attention coefficients  $\alpha_{v_i, v_j}^h$  are computed according to Eq. (4)

$$\alpha_{v_i, v_j}^h = \frac{e^{\epsilon_{v_j}^h}}{\sum_{v_k \in \mathcal{N}(v_i) \cup \{v_i\}} e^{\epsilon_{v_k}^h}} \quad (4)$$

where  $\epsilon_{v_w}^h = \mathbf{a}^h \top \text{LeakyReLU}(\Theta_s^h \mathbf{x}_{v_i} + \Theta_t^h \mathbf{x}_{v_w})$ ,  $\Theta_s^h$  is the transformation matrix for source nodes, and  $\mathbf{a}^h$  is the learnable attention vector. A second GATv2 layer refines these embeddings using a single attention head producing the embedding  $\mathbf{x}_{v_i}^{(2)}$  as per Eq. (5).

$$\mathbf{x}_{v_i}^{(2)} = \sum_{v_j \in \mathcal{N}(v_i) \cup \{v_i\}} \alpha_{v_i, v_j} \mathbf{W} \mathbf{x}_{v_j}^{(1)} \quad (5)$$

where  $\mathbf{W}$  is the learned projection matrix.

The exploration policy and critic network both process the node features  $v_{out} = \{v_a\} \cup \mathcal{V}_n$  representing the learned ranking of candidate waypoints. The policy outputs the features of these nodes, while the critic aggregates the features and applies a fully connected layer.

#### D. Reward Shaping with Frontier-based Potential Field

The reward function used to train the exploration greedy policy  $\pi_\theta$  is formulated to encourage efficient exploration and penalize the intervention of the safety shield requested to avoid collisions. Therefore, the reward  $r_t(s_t, a_t^\pi, a_t^\sigma, s_{t+1})$  is defined according to Eq. (6):

$$r_t = \begin{cases} r_{exp}, & \text{if } \rho_t \geq \rho^* \text{ and } a_t^\pi = a_t^\phi \\ n_t^e + \Phi(s_{t+1}) - \Phi(s_t), & \text{if } \rho_t < \rho^* \text{ and } a_t^\pi = a_t^\phi \\ r_\sigma, & \text{if } a_t^\pi \neq a_t^\phi \end{cases} \quad (6)$$

where  $n_t^e$  is the number of explored cells added to the agent's map at time step  $t$  due to the execution of  $a_t^\sigma$ , and  $\Phi(\cdot)$  is the function computing the frontier-based potential field. This map evaluates the current state of exploration  $s_t$  by considering both the spatial distances of the frontiers from the agent position  $x_t^a$  and the expected information gain of these frontiers. In particular, given a set of frontiers  $\mathcal{F}_t = \{f_1, f_2, \dots, f_n\}$ , where each  $f_i$  represents the coordinates of a frontier, the distances between the current position of the agent  $x_t^a$  and each frontier are computed according to Eq. (7):

$$d_i = \|f_i - x_t^a\|_2 \quad (7)$$

and  $\bar{d}_i$  corresponds to the value of  $d_i$  scaled in the range  $[0, 1]$ . The expected information gain for each frontier  $f_i$  is then computed based on the number of unknown grid cells in a local region  $\mathcal{N}$  around each frontier of size  $k \times k$  according to Eq. (8).

$$\Gamma_i = \sum_{x \in \mathcal{N}(f_i)} \gamma(x) \quad (8)$$

where  $\gamma(\cdot)$  is the function that counts unknown cells in the neighbor  $\mathcal{N}$ , and  $\bar{\Gamma}_i$  corresponds to the value of  $\Gamma_i$  scaled in the range  $[0, 1]$ . Then the potential field  $\Phi_i$  associated with each frontier is computed according to Eq. 9 as a linear combination of the distances and information gains and the trade-off between these two factors is controlled by a parameter  $\beta$ .

$$\Phi_i = -\bar{d}_i + \beta \cdot \bar{\Gamma}_i \quad (9)$$

The potentials are then normalized again to ensure they lie within the range  $[0, 1]$ :

$$\bar{\Phi}_i = \frac{\Phi_i + 1}{\beta + 1}$$

Finally, the frontier potential in state  $s_t$  is determined as the maximum potential across all frontiers.

### III. SIMULATION

#### A. Training Setup

The training was conducted on HPC2N's Kebnekaise cluster running Ubuntu 20.04.6 LTS, utilizing 5 Skylake CPU cores and an NVIDIA H100 GPU, while policy evaluations were performed on the same system using 10 Skylake CPU cores. The environment was implemented using Gymnasium [32], with the key design parameters summarized in Table II. The exploration policy and critic were modeled using a graph-based neural network implemented in PyTorch Geometric [33]. Training was performed in environments with varying non-traversable region distributions and initial agent placements to enhance policy generalization. The PPO algorithm was implemented using skrl [34], with the key hyperparameters detailed in Table II. Moreover, the reward function is designed considering  $r_{exp} = 100$ ,  $r_\sigma = -5$  and  $\beta = 0.5$ . Fig. 3-(a) shows the mean total reward curve collected during the training after having performed a smoothing and a scaling of the obtained rewards in the range  $[0, 1]$ . It can be seen that the rewards generally increase except for a small decline after  $6 \times 10^4$  steps from the beginning of the training. Nevertheless, the graph demonstrates that the reward curve converges.

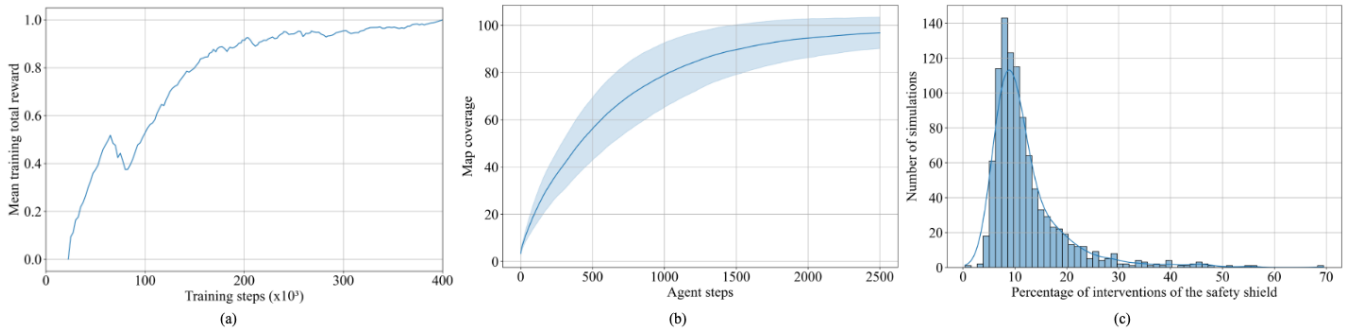


Fig. 3. From left to right: (a) Mean total reward curve during training, smoothed and scaled to  $[0, 1]$ . (b) Map coverage percentage relative to traversable regions over agent steps in 1000 test environments. (c) Distribution of the percentages of safety shield interventions over agent actions across 1000 test simulations.

TABLE II  
PARAMETERS USED FOR ENVIRONMENT AND TRAINING SETUP

Environment		Training	
Name	Value	Name	Value
$h, w$	50	Rollouts	1024
$n_t$	45	Mini-Batches	64
$r_t$	$[1, 3]$	Learning Rate	$3 \times 10^{-4}$
$l$	5.0	Learning Epochs	8
$\rho^*$	0.98	Discount factor $\gamma$	0.99
$n_s^*$	2500	Training timesteps	$4 \cdot 10^5$
$k$	7	Clipping parameter $\epsilon$	0.2

### B. Simulation Results

The policy trained with the parameters in Table II is evaluated in 1000 test environments with randomly placed non-traversable regions and agent starting positions. The framework, consisting of an RL-based greedy exploration policy and a safety shield, is executed for 2500 time steps to assess its robustness across different environment configurations.

Figure 3-(b) illustrates the average map coverage over agent steps during exploration. The results show a steady increase in coverage, reaching 80% after 1000 steps and approximately 95% after 2000 steps. This demonstrates the framework’s capability to achieve high exploration efficiency despite variations in environment configurations. Additionally, Figure 3-(c) presents the percentage of the number of steps in which the safety shield intervenes to avoid a collision

over the total number of actions per simulation, showing that in 80% of simulations, interventions occur in less than 15% of steps, with an average intervention rate of around 10%. This demonstrates that the policy effectively explores with minimal reliance on the safety shield. However, its utility is evident during execution, as it is occasionally activated when necessary.

To further analyze robustness, the proposed approach is tested in environments with varying numbers of trees and different map sizes. In the first case, 1000 simulations are conducted, each running for 2500 steps, while in the second case, 100 simulations are executed for 10,000 steps. In particular, Fig. 4-(a) demonstrates the policy’s adaptability to different environment sizes. The agent successfully explores more than 80% of the traversable area after approximately 2500 steps in maps 125% larger than the nominal size and after 5000 steps in maps 300% larger. Moreover, Fig. 4-(b) shows that while an increase in non-traversable regions slightly reduces map coverage considering the same number of agent steps, the policy still achieves over 80% coverage even with a 67% increase in the number of trees. The increased obstacle complexity is also reflected in Figure 4-(c), where the safety shield activates more frequently as the number of trees grows. This highlights the necessity of the safety module in ensuring safe exploration. However, even in the most complex configurations, the policy maintains the intervention rate around 20% of the total exploration

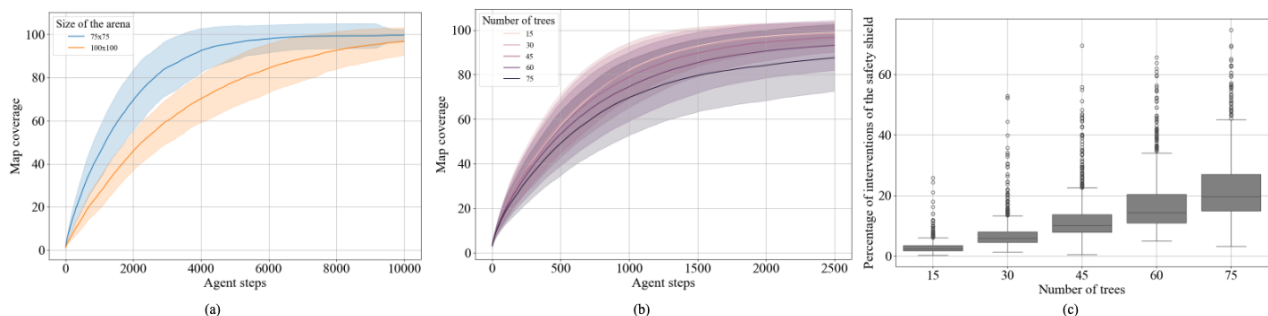


Fig. 4. From left to right: (a)–(b) Map coverage percentage over agent steps in environments with varying sizes of the exploration arena and non-traversable regions. (c) Distribution of safety shield intervention ratio across agent actions for different tree densities.

steps. These results confirm the framework’s scalability and robustness in diverse exploration scenarios.

#### IV. CONCLUSIONS

This paper presents a novel framework for safe and efficient exploration in cluttered environments, simulating forest scenarios where an unmanned aerial vehicle navigates between tree trunks. The proposed strategy employs a graph neural network with attention, trained via reinforcement learning, to optimize exploration while minimizing the need for a safety shield to intervene in the navigation controller. Additionally, a new graph-based representation of relevant locations and a frontier-based potential field reward term are introduced to prioritize movement toward high-gain frontiers while minimizing distance from the agent. Experimental results demonstrate robust map coverage across diverse environmental configurations, with the safety shield intervening less than 10% of the time. The framework’s robustness is further validated through tests with varying tree numbers and environmental sizes. Future works will focus on implementing this framework as a high-level exploration planner in a real unmanned aerial vehicle to explore a real-world forest.

#### REFERENCES

- [1] S. Amin, M. Gomrokchi, H. Satija, H. Van Hoof, and D. Precup, “A survey of exploration methods in reinforcement learning,” *arXiv preprint arXiv:2109.00157*, 2021.
- [2] L. C. Garaffa, M. Basso, A. A. Konzen, and E. P. de Freitas, “Reinforcement learning for mobile robotics exploration: A survey,” *IEEE Transactions on Neural Networks and Learning Systems*, vol. 34, no. 8, pp. 3796–3810, 2021.
- [3] M. Hutsebaut-Buyssse, K. Mets, and S. Latré, “Hierarchical reinforcement learning: A survey and open research challenges,” *Machine Learning and Knowledge Extraction*, vol. 4, no. 1, pp. 172–221, 2022.
- [4] B. Singh, R. Kumar, and V. P. Singh, “Reinforcement learning in robotic applications: a comprehensive survey,” *Artificial Intelligence Review*, vol. 55, no. 2, pp. 945–990, 2022.
- [5] S. Pateria, B. Subagdjia, A.-h. Tan, and C. Quek, “Hierarchical reinforcement learning: A comprehensive survey,” *ACM Computing Surveys (CSUR)*, vol. 54, no. 5, pp. 1–35, 2021.
- [6] P. Ladosz, L. Weng, M. Kim, and H. Oh, “Exploration in deep reinforcement learning: A survey,” *Information Fusion*, vol. 85, pp. 1–22, 2022.
- [7] Y. Xue and W. Chen, “A uav navigation approach based on deep reinforcement learning in large cluttered 3d environments,” *IEEE Transactions on Vehicular Technology*, vol. 72, no. 3, pp. 3001–3014, 2022.
- [8] R. Cimurs, I. H. Suh, and J. H. Lee, “Goal-driven autonomous exploration through deep reinforcement learning,” *IEEE Robotics and Automation Letters*, vol. 7, no. 2, pp. 730–737, 2021.
- [9] Y. Cao, T. Hou, Y. Wang, X. Yi, and G. Sartoretti, “Ariadne: A reinforcement learning approach using attention-based deep networks for exploration,” in *2023 IEEE International Conference on Robotics and Automation (ICRA)*. IEEE, 2023, pp. 10 219–10 225.
- [10] C. Sun, J. Orbik, C. M. Devin, B. H. Yang, A. Gupta, G. Berseth, and S. Levine, “Fully autonomous real-world reinforcement learning with applications to mobile manipulation,” in *Conference on Robot Learning*. PMLR, 2022, pp. 308–319.
- [11] Q. Liu, X. Li, Y. Tang, X. Gao, F. Yang, and Z. Li, “Graph reinforcement learning-based decision-making technology for connected and autonomous vehicles: Framework, review, and future trends,” *Sensors*, vol. 23, no. 19, p. 8229, 2023.
- [12] S. Munikoti, D. Agarwal, L. Das, M. Halappanavar, and B. Natarajan, “Challenges and opportunities in deep reinforcement learning with graph neural networks: A comprehensive review of algorithms and applications,” *IEEE transactions on neural networks and learning systems*, 2023.
- [13] M. Nie, D. Chen, and D. Wang, “Reinforcement learning on graphs: A survey,” *IEEE Transactions on Emerging Topics in Computational Intelligence*, vol. 7, no. 4, pp. 1065–1082, 2023.
- [14] Z. Zhang, C. Shi, P. Zhu, Z. Zeng, and H. Zhang, “Autonomous exploration of mobile robots via deep reinforcement learning based on spatiotemporal information on graph,” *Applied Sciences*, vol. 11, no. 18, p. 8299, 2021.
- [15] E. P. Herrera-Alarcón, G. Baris, M. Satler, C. A. Avizzano, and G. Loianno, “Learning heuristics for efficient environment exploration using graph neural networks,” in *2023 21st International Conference on Advanced Robotics (ICAR)*. IEEE, 2023, pp. 86–93.
- [16] F. Yang, X. Li, Q. Liu, Z. Li, and X. Gao, “Generalized single-vehicle-based graph reinforcement learning for decision-making in autonomous driving,” *Sensors*, vol. 22, no. 13, p. 4935, 2022.
- [17] Y. Lu, Y. Chen, D. Zhao, and D. Li, “Mgrl: Graph neural network based inference in a markov network with reinforcement learning for visual navigation,” *Neurocomputing*, vol. 421, pp. 140–150, 2021.
- [18] S. Gu, L. Yang, Y. Du, G. Chen, F. Walter, J. Wang, and A. Knoll, “A review of safe reinforcement learning: Methods, theories and applications,” *IEEE Transactions on Pattern Analysis and Machine Intelligence*, 2024.
- [19] L. Brunke, M. Greeff, A. W. Hall, Z. Yuan, S. Zhou, J. Panerati, and A. P. Schoellig, “Safe learning in robotics: From learning-based control to safe reinforcement learning,” *Annual Review of Control, Robotics, and Autonomous Systems*, vol. 5, no. 1, pp. 411–444, 2022.
- [20] W. Zhao, T. He, R. Chen, T. Wei, and C. Liu, “State-wise safe reinforcement learning: A survey,” *arXiv preprint arXiv:2302.03122*, 2023.
- [21] M. Xu, Z. Liu, P. Huang, W. Ding, Z. Cen, B. Li, and D. Zhao, “Trustworthy reinforcement learning against intrinsic vulnerabilities: Robustness, safety, and generalizability,” *arXiv preprint arXiv:2209.08025*, 2022.
- [22] M. Guerrier, H. Fouad, and G. Beltrame, “Learning control barrier functions and their application in reinforcement learning: A survey,” *arXiv preprint arXiv:2404.16879*, 2024.
- [23] J. Achiam, D. Held, A. Tamar, and P. Abbeel, “Constrained policy optimization,” in *International conference on machine learning*. PMLR, 2017, pp. 22–31.
- [24] L. Yang, J. Ji, J. Dai, Y. Zhang, P. Li, and G. Pan, “Cup: A conservative update policy algorithm for safe reinforcement learning,” *arXiv preprint arXiv:2202.07565*, 2022.
- [25] W. Huang, J. Ji, C. Xia, B. Zhang, and Y. Yang, “Safedreamer: Safe reinforcement learning with world models,” *arXiv preprint arXiv:2307.07176*, 2023.
- [26] S. Feng, H. Sun, X. Yan, H. Zhu, Z. Zou, S. Shen, and H. X. Liu, “Dense reinforcement learning for safety validation of autonomous vehicles,” *Nature*, vol. 615, no. 7953, pp. 620–627, 2023.
- [27] J. Dai, J. Ji, L. Yang, Q. Zheng, and G. Pan, “Augmented proximal policy optimization for safe reinforcement learning,” in *Proceedings of the AAAI Conference on Artificial Intelligence*, vol. 37, no. 6, 2023, pp. 7288–7295.
- [28] L. Zhang, Q. Zhang, L. Shen, B. Yuan, X. Wang, and D. Tao, “Evaluating model-free reinforcement learning toward safety-critical tasks,” in *Proceedings of the AAAI conference on artificial intelligence*, vol. 37, no. 12, 2023, pp. 15 313–15 321.
- [29] Y. J. Ma, A. Shen, O. Bastani, and J. Dinesh, “Conservative and adaptive penalty for model-based safe reinforcement learning,” in *Proceedings of the AAAI conference on artificial intelligence*, vol. 36, no. 5, 2022, pp. 5404–5412.
- [30] J. Schulman, F. Wolski, P. Dhariwal, A. Radford, and O. Klimov, “Proximal policy optimization algorithms,” 2017. [Online]. Available: <https://arxiv.org/abs/1707.06347>
- [31] S. Brody, U. Alon, and E. Yahav, “How attentive are graph attention networks?” 2022. [Online]. Available: <https://arxiv.org/abs/2105.14491>
- [32] M. Towers, A. Kwiatkowski, J. Terry, J. U. Balis, G. De Cola, T. Deleu, M. Goulão, A. Kallinteris, M. Krimmel, A. KG *et al.*, “Gymnasium: A standard interface for reinforcement learning environments,” *arXiv preprint arXiv:2407.17032*, 2024.
- [33] M. Fey and J. E. Lenssen, “Fast graph representation learning with PyTorch Geometric,” in *ICLR Workshop on Representation Learning on Graphs and Manifolds*, 2019.
- [34] A. Serrano-Muñoz, D. Chrysostomou, S. Bøgh, and N. Arana-Arexolaleiba, “skrl: Modular and flexible library for reinforcement learning,” *Journal of Machine Learning Research*, vol. 24, no. 254, pp. 1–9, 2023.